



Effect of reservoir models and climate change on flood analysis in arid regions

Ahmed samy Kamis¹ · Abdullah Al-Wagdany¹ · Jarbou Bahrawi¹ · Muhammad Latif² · Amro Elfeki¹ · Abdel Hannachi³

Received: 31 December 2019 / Accepted: 29 July 2020 / Published online: 19 August 2020
© Saudi Society for Geosciences 2020

Abstract

Dams are built in arid regions across watersheds for flood control among other purposes. Capacity-elevation (C-E) curves are vital for reservoir routing and dam operation. Different models are available for representing C-E relationships. Power and logarithmic laws are evaluated and tested for reservoir routing. The evaluation is based on the analysis of 136 reservoirs across different regions of Saudi Arabia (SA). The analysis revealed that 75.7% of the reservoirs are of flood plain foothill type. A case study on Al-Lith dam basin is utilized for application based on measured events. The resulting routed outflow hydrographs showed that the logarithmic law is better to represent the reservoir than the power law. With respect to the climate change effect, the results show that the predicted rainfall from Representative Concentration Pathways scenario (RCP4.5) increased by about 20 to 31.4% from 5 to 100 years return periods respectively with an average of 27%. While for scenario RCP8.5, the predicted rainfall increased by 42% to about 55% from 5 to 100 years return periods respectively with an average of 49%. For the RCP4.5 scenario, the peak flows, Q_p , and volumes, W , increased by an average of 69% and 67% respectively. While for the RCP8.5 scenario, the same parameters increased by an average of 139% and 134% respectively. The effect of transmission losses in the results seems to be minor with respect to climate change signal (for RCP4.5, Q_p and W are lowered on average by 2% and 0.5% respectively, and for RCP8.5, Q_p and W are lowered on average by 4.5% and 1.3% respectively). The results of this research recommend to use the logarithmic law and to take into account the effect of climate change on future dam projects in SA.

Keywords Reservoir model · Climate change · Infrastructures · Routing · Transmission losses

Introduction

In arid regions of Saudi Arabia (SA), the main infrastructures to combat flash floods are dams and flood channels. The design of such structures depends on the analysis of recorded storms. However, recorded hydrographs are rare. Empirical

equations and software are used to generate the inflow hydrograph for the design of dams and the sizing of the reservoirs. Flood routing is then used to generate outflow hydrographs for the design of flood (emergency) channels. Flood routing requires information about the morphology of the reservoir. Several methods are available for the representation of reservoir morphology. Macchione et al. (2016) introduced simple power law to represent the relationship between the reservoir volume and the water depth. Their equation reads as follows:

$$W(Z) = W_0 Z^{\alpha_0} \quad (1)$$

where $W(Z)$ is the volume at water depth Z , and W_0 and α_0 are parameters obtained by the method of least squares. They applied the above, Eq. (1), to 97 reservoirs in different geographical areas in the world. Mohammadzadeh-Habibi et al. (2009) and Haghiabi et al. (2013) presented

Responsible Editor: Broder J. Merkel

✉ Ahmed samy Kamis
akamis@kau.edu.sa; samyzaheer@yahoo.com

¹ Department of Hydrology and Water Resources Management, Faculty of Meteorology, Environment, and Arid Land Agriculture, King Abdulaziz University, P.O. Box 80208, Jeddah 21589, Kingdom of Saudi Arabia

² Department of Meteorology, COMSATS University Islamabad (CUI), Islamabad 45550, Pakistan

³ Department of Meteorology, Stockholm University, Stockholm, Sweden

a logarithmic law to represent the relationship between reservoir volume and the depth. The equation reads as follows:

$$W(Z) = W_{\max} \left(e^{\ln(2) \frac{Z}{Z_{\max}}} - 1 \right)^{\frac{1}{N}}, \quad (2)$$

where W_{\max} is the maximum volume of the reservoir, Z_{\max} is the maximum water depth, and N is the reservoir coefficient, which can be calculated using the following equation:

$$N = 2 \ln(2) \frac{W_{\max}}{A_{\max} Z_{\max}} \quad (3)$$

where A_{\max} is the maximum surface area of the reservoir.

The above authors applied Eqs. (2) and (3) to eight reservoirs in Iran and showed that the equation represents the reservoirs well. Rahmanian and Banihashemi (2012) used Eq. (2) to study the sediment distribution in reservoirs. Their results suggest the applicability of the equation for the nine reservoirs selected for their study.

Reservoir routing is a process where inflow hydrograph is attenuated as it passes through a dam outlet or spillway. Numerous studies have been undertaken to calculate the outflow hydrograph for the design of the flood channel downstream of the dam. Most of those studies were conducted for river management. Few studies were directed towards arid region conditions where reservoirs in most cases are empty. Therefore, the reservoir morphology must be taken into account in the calculation of the reservoir routing (Kamis et al. 2018).

Climate change studies are based on global models run under different types of climate scenarios of CO₂ emissions. The results of these climate models are used to obtain regional results through downscaling experiments. The regional results can also be used to obtain information on local scale through another downscaling process. Monier and Gao (2015) presented a study regarding the expected extreme hot or extreme precipitation that would occur in the USA over the twenty-first century using the MIT global model. The model predictions show that extreme precipitations are expected in much higher frequency than predictions, based on the historical records. Ambjerg-Nielsen (2012) examined the effect of climate change on rainfall intensities. The analysis was based on the historical precipitation records and a regional climate model. Two approaches were employed and the results showed that the rainfall intensities in Denmark would increase by 10–50% by the end of twenty-first century. Elshorbagy et al. (2018) presented a study to appraise the effect of climatic change in relation to the design of urban storm water facilities (detention ponds). The study explored several scenarios of rainfall storms on the existing facilities. Their results showed that under climate change scenarios, the runoff volume would exceed the design parameters of the detention ponds.

In a study by Chowdhury and Al-Zahrany (2013), the long-term prediction of climatic parameters was investigated. Results of the HadCAM3 (Rajab and Prudhomme 2002) global model were utilized to predict the influence of climatic change on the water resources up to year 2050. Their results showed that precipitation would increase by about 20% by year 2050 on the western region of SA.

Through the aforementioned review, it is of great importance to test the readiness of the current flood protection infrastructures to the climate change effects; therefore, the objectives of this study are two-fold:

- (1) To develop the appropriate relationship between reservoir volume and water depth for evaluating the outflow hydrograph of the dam that is relevant to the prevailing conditions in arid regions.
- (2) To predict the expected storms due to climate change for evaluating the risk on the existing flood mitigation infrastructures.

In the current study, an investigation of the appropriate method for representing reservoir morphology is carried out. The most recent (Sep. 2014) digital elevation data (digital elevation model (DEM)), which were used for the 136 watersheds, were downloaded from the U.S. Geological Survey (USGS) to estimate the reservoir morphology: the reservoir-capacity and area-capacity curves. The 136 reservoirs are distributed across different regions of SA. The study further explores the effect of climate change on the expected future storms that in turn will affect the design and operation of flood mitigation infrastructures. A comprehensive study of Al-Lith watershed was conducted for 4 years (Dames and Moore 1988). Precisely, rainfall records along with runoff gauge records were collected at several stations along the watershed. The recorded data at Al-Lith dam (under construction) will be employed as input for the reservoir routing. The outflow hydrographs, based on two reservoir models, will be tested against each other and against the traditional Plus method to find out any significant difference between them. The study looks further for the effect of climate change on the outflow hydrographs.

Reservoir morphology

In order to investigate the method for representing the morphology of a reservoir, comprehensive data collection from 136 reservoirs, distributed over SA, are conducted from DEM. Some of these dams are operational and the rest are either under design study or under construction. Figure 1 shows the locations of these dams throughout the region. Reservoirs can be classified by several methods. In this study, the classification introduced by Borland and Miller (1958) is adopted as shown in Table 1. In this table, M is known as the reservoir shape

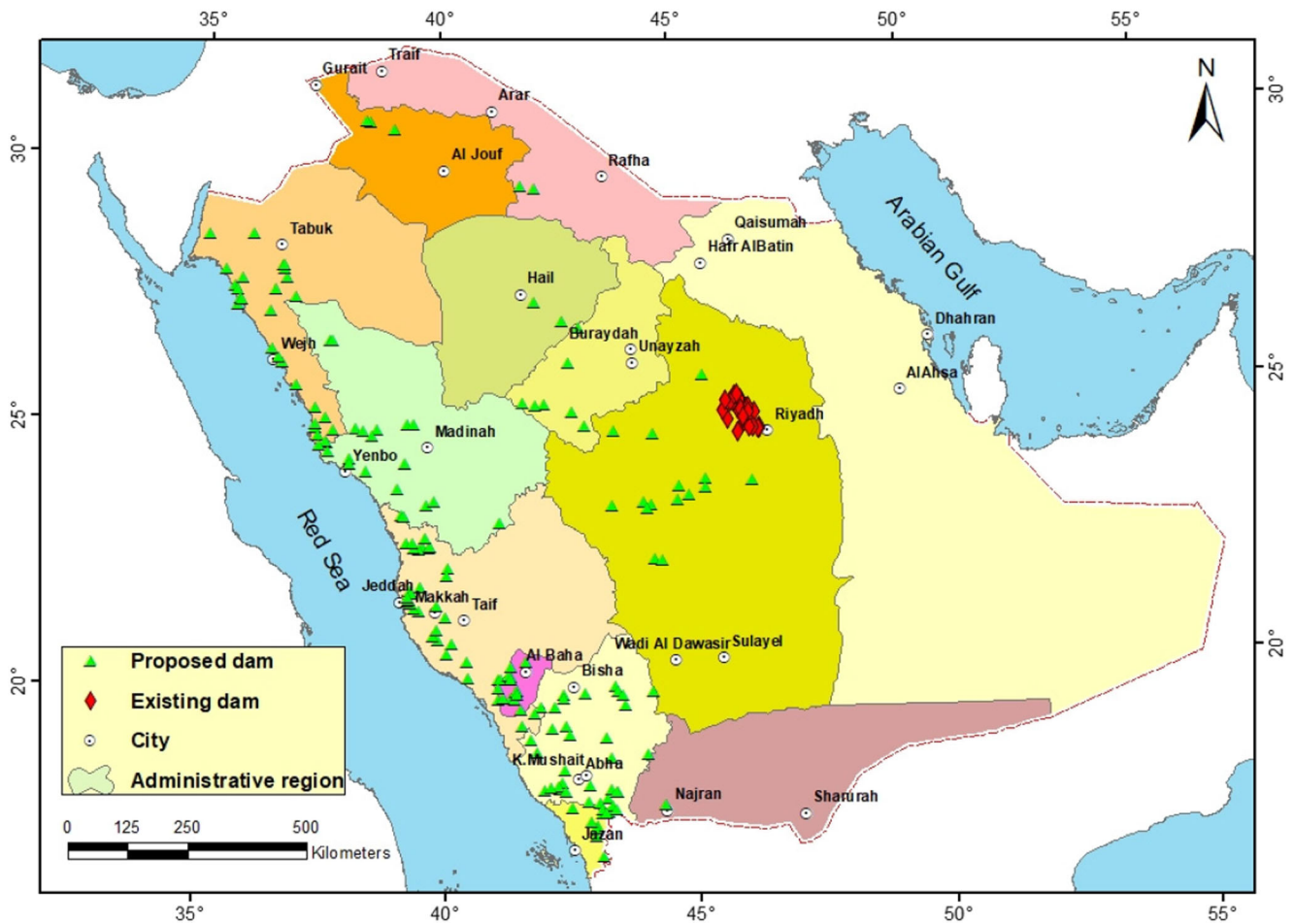


Fig. 1 Locations of dams used in the current study

factor. This factor is related to the reservoir coefficient N (Eq. (3)) according to the following relation as explained by Mohammadzadeh-Habili et al. (2009):

$$N = 1.075 M^{-0.9063} \tag{4}$$

Table 2 shows the distribution of reservoirs among the various regions of SA according to Borland and Miller (1958). The table shows that the majority of the reservoirs fall under class III.

The DEM data were used to calculate the volume of the reservoir as a function of the depth using Eqs. (1–3) in order to

compare the two methods of modeling the morphology of the reservoirs. Simple statistical analysis is employed to assess the suitability of the two methods by calculating the coefficient of determination R^2 . In addition, the percentage of error E_W is calculated based on the following equation:

$$E_W = \frac{W_c - W_m}{W_m} \times 100\% \tag{5}$$

where W_c is the calculated volume from the equation, and W_m is the measured volume from the data (DEM).

Figure 2a, b shows a comparison of the distribution of the percentage of errors for both models for the different regions of the study area. Table 3 shows the results of the fitting parameters of both reservoir models. The results show that both methods produce very good agreement with the measured data. However, the overall R^2 for the logarithmic law is higher than that for the power method.

Figure 2a, b shows that for most regions, the range of the percentage of error for the logarithmic method lies between -4 and $+8\%$, while for the power method, the range is observed between -50 and $+5\%$. Another measure of comparison is

Table 1 Classification of reservoirs

M	Reservoir type	Standard classification
3.5–4.5	Gorge	I
2.5–3.5	Hill	II
1.5–2.5	Flood plain foothill	III
1.0–1.5	Lake	IV

Table 2 Classification of reservoirs in the study region

Region	Classification of reservoirs				Total
	I ($M = 3.5-4$)	II ($M = 2.5-3.5$)	III ($M = 1.5-2.5$)	IV ($M = 1-1.5$)	
Riyadh	1	5	20	4	30
Makkah	0	2	18	0	20
Madinah	0	6	19	0	25
Baha-Najran-Jizan	0	1	11	1	13
Aseer	0	6	26	0	32
Tabouk-Hail	0	8	8	0	16
KSA	1	28	102	5	136
%	0.74	20.5	75.1	3.66	100

the percentage of relative root mean square error (%RRMSE) that is calculated as follows:

$$\%RRMSE = \frac{RMSE}{\bar{W}} \times 100 \tag{6}$$

where \bar{W} is the mean of the measured volume of the reservoir, and the root mean square error is given by:

$$RMSE = \sqrt{\frac{\sum_{i=1}^n (w_i - c_i)^2}{n}} \tag{7}$$

where w_i is the measured volume at elevation i and c_i is the calculated volume (from the model) at the same elevation i . Li et al. (2013) proposed that the model accuracy is considered excellent when $\%RRMSE < 10\%$, fair if $20\% < \%RRMSE < 30\%$, and poor if $\%RRMSE \geq 30\%$.

Table 3 shows that the range of the %RRMSE for the logarithmic method lies between 5.1 and 7.7% with an average of 6.6% (classified as excellent), while for the power method, the range is between 15 and 24.9% with an average of 22.7% (classified as fair). These results clearly indicate that the logarithmic model performs better compared to the power law model.

Reservoir routing

The following equations are reservoir routing equations in terms of power and logarithmic representation of the reservoir morphology. The derivations of these equations are presented in the Appendix.

$$\frac{dZ}{dt} = \frac{I(t) - CB(Z - P)^{1.5}}{\alpha_o W_o Z^{\alpha_o - 1}} \tag{8}$$

$$\frac{dZ}{dt} = \frac{I(t) - CB(Z - P)^{1.5}}{\left[\frac{S_{max} \ln(2)}{NZ_{max}} e^{(\ln 2) \left(\frac{Z}{Z_{max}} \right)} \left(e^{(\ln 2) \left(\frac{Z}{Z_{max}} \right)} - 1 \right)^{(1-N)/N} \right]} \tag{9}$$

Equations (8) and (9) are differential equations that do not have readily analytical solutions. A numerical solution is then used. A forward Euler finite difference scheme is used to obtain a numerical solution (Kamis et al. 2018). The outflow hydrograph is deduced once the inflow hydrograph, reservoir characteristics, and the spillway parameters are available. To assess the accuracy of the two methods of representing the reservoir morphology, the traditional method of reservoir routing is employed. Chow et al. (1988) introduced the traditional (modified Plus or reservoir indicator method) equation that can be written as follows:

$$\frac{W(t + \Delta t) - W(t)}{\Delta t} = \frac{I(t + \Delta t) + I(t)}{2} - \frac{O(t + \Delta t) + O(t)}{2} \tag{10}$$

where $W(t + \Delta t)$ is the reservoir storage at time $t + \Delta t$, $W(t)$ is the reservoir storage at time t , Δt is time increment, $I(t + \Delta t)$ is inflow at time $t + \Delta t$, $I(t)$ is inflow at time t , $O(t + \Delta t)$ is outflow at time $t + \Delta t$, and $O(t)$ is outflow at time t .

This equation can be rearranged as follows:

$$I(t + \Delta t) + I(t) + \left[\frac{2W(t)}{\Delta t} - O(t) \right] = \frac{2W(t + \Delta t)}{\Delta t} + O(t + \Delta t) \tag{11}$$

In this equation, only unknown terms for any time interval are the terms on the right-hand side. In order to evaluate the outflow $O(t + \Delta t)$, a storage indication curve (storage–outflow) relating $O(t + \Delta t)$ and $2W(t + \Delta t)/\Delta t +$

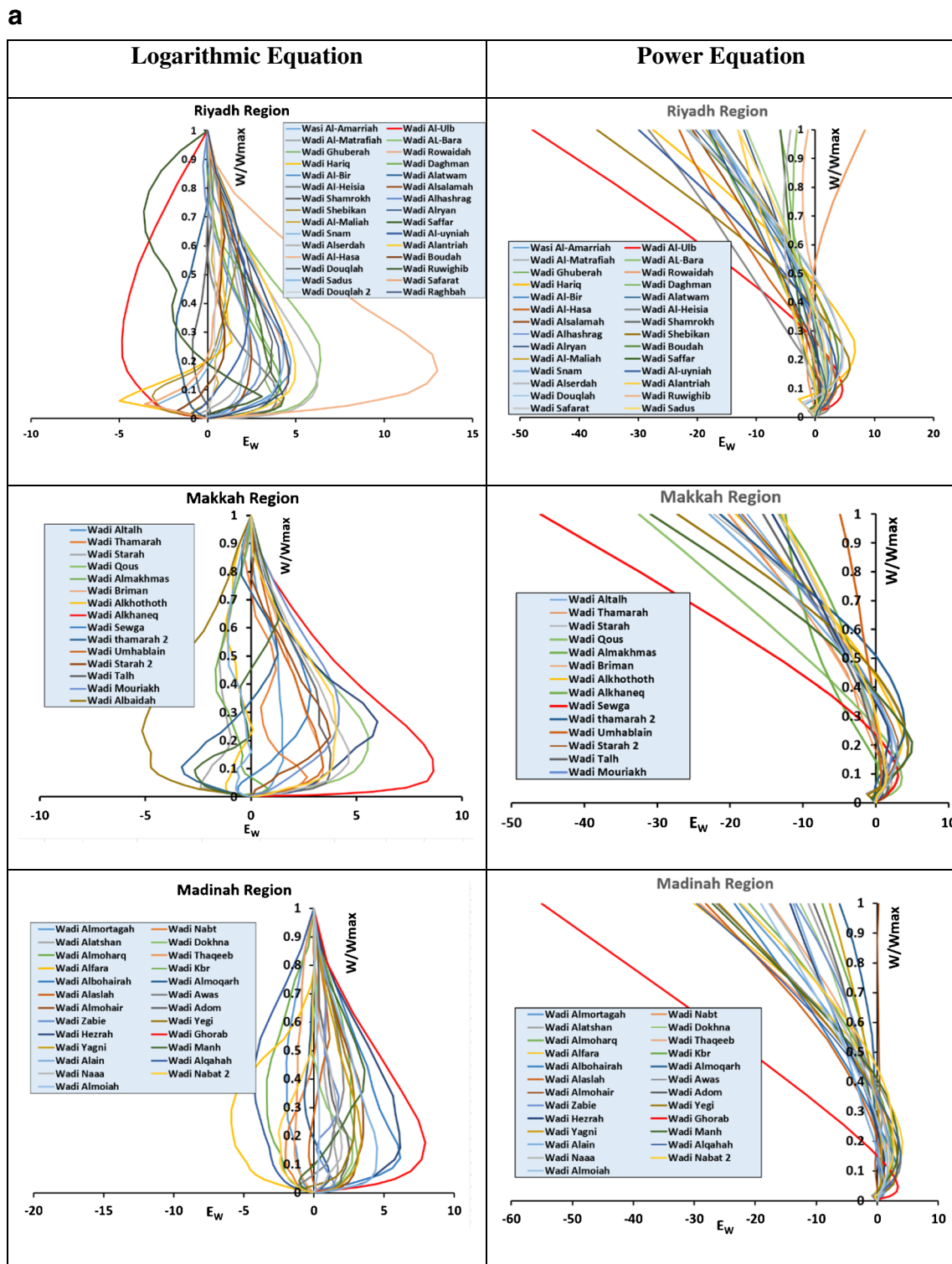


Fig. 2 a Comparison of % E_w between two reservoir models in different regions of KSA (Riyadh, Makkah, and Madinah). **b** Comparison of % E_w between two reservoir models in different regions of KSA (Baha-Najran-Jizan, Aseer, and Tabouk-Hail)

$O(t + \Delta t)$ is required. At any reservoir elevation, the storage is known from topographic data and the outflow can be calculated from the spillway governing equation.

Hence, a relation between the outflow $O(t)$ and $(2W(t)/\Delta t + O(t))$ is obtained in a tabular form or graphically. In routing the flow through time step $(t + \Delta t)$, the left-

b

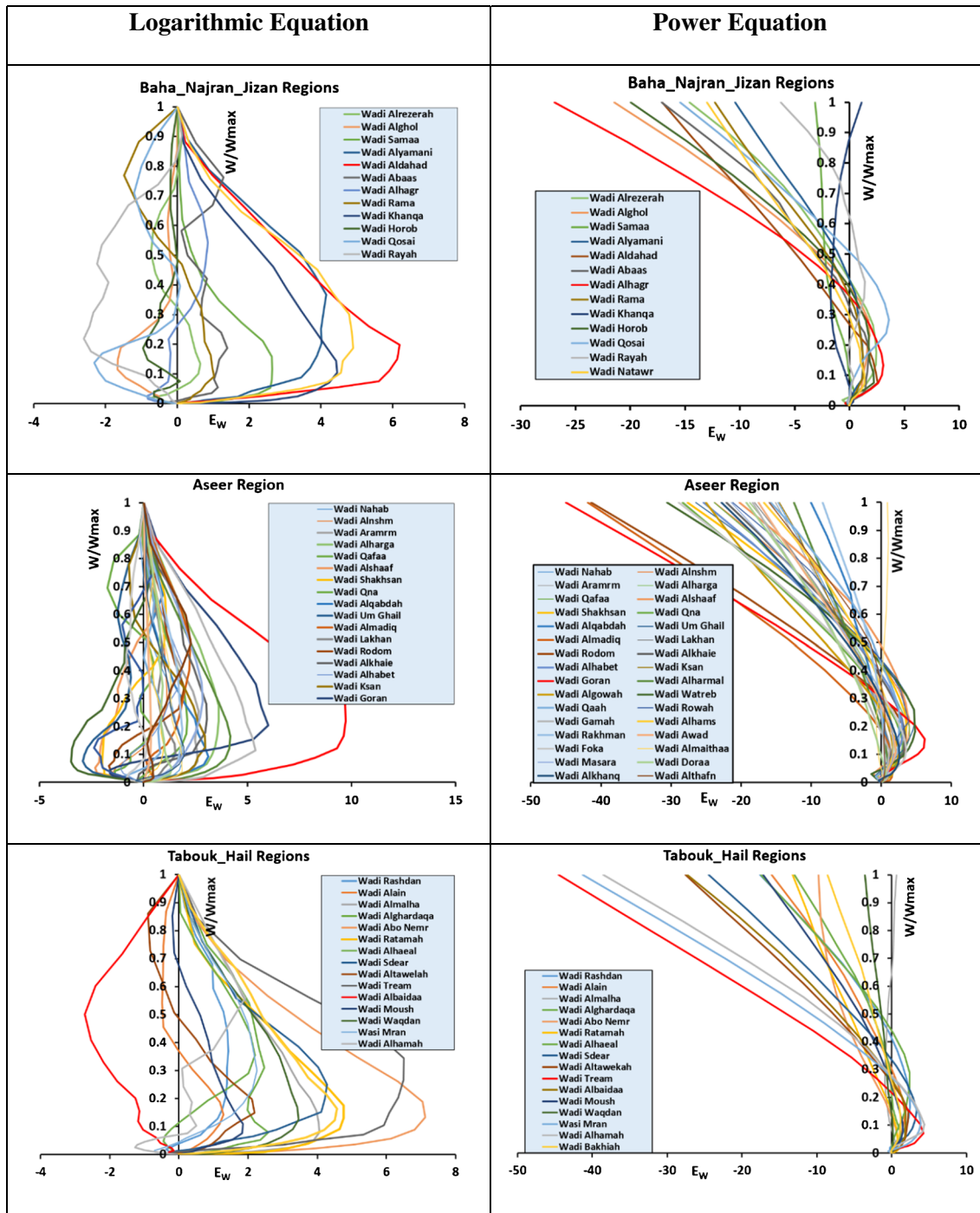


Fig. 2 continued.

hand side of Eq. (11) is evaluated to give the value of the right-hand side of the equation. Then, from the former established relation, by interpolation using tables or regression of the graphical relation, the outflow $O(t + \Delta t)$ is obtained. An Excel sheet has been developed to solve Eqs. (8), (9), and (11) (Kamis et al. 2018).

Al-Lith dam case study

Wadi Al-Lith is located in the western part of SA. It is located about 200 km south of Jeddah city. It lies between $40^{\circ} 10'$ and $40^{\circ} 50'$ longitudes and $20^{\circ} 00'$ and $21^{\circ} 15'$ latitudes with an area about 3262 km^2 as shown in Fig. 3. Wadi Al-

Table 3 Comparison between the fitting parameters of the reservoir models (logarithmic and power laws) and the estimation errors

Region	Logarithmic equation					Power equation										
	%RRSME		R^2		N	M		R^2		W_0	α_0					
	Average	Max.	Average	Min.	Average	Max.	Min.	Average	Max.	Average	Max.	Min.				
Riyadh	7.7	0.9987	0.59	0.83	0.33	2.03	3.66	1.32	24.8	0.9716	111,393	556,104	1202	2.05	3.45	1.04
Makkah	7.0	0.9991	0.56	0.68	0.35	2.09	3.49	1.65	23.3	0.9771	37,427	213,731	2420	1.97	2.49	1.27
Madinah	6.9	0.9981	0.52	0.61	0.37	2.26	2.56	1.81	23.0	0.9806	28,967	159,992	1902	2.12	2.69	1.42
Baha-Najran-Jizan	5.1	0.9994	0.59	0.76	0.48	1.97	2.50	1.47	15.0	0.9895	11,834	40,417	3735	2.00	2.84	1.46
Aseer	5.7	0.9993	0.54	0.74	0.37	2.22	3.25	1.51	24.9	0.9752	38,803	309,317	1486	2.05	3.10	1.23
Tabouk-Hail	7.0	0.9990	0.52	0.76	0.42	2.30	2.79	1.47	24.9	0.9756	59,519	623,005	1935	2.25	3.51	1.7
KSA	6.6	0.9991	0.55	0.83	0.33	2.15	3.66	1.32	22.7	0.9783	47,991	0.9057	2113	2.07	3.02	1.35

Lith consists of five sub-basins. Between 1984 and 1988, Dames & Moore, a US company, conducted a comprehensive project on water resources in selected regions of SA. The study area is located in one of these regions; thus, we collected the required data from the reports of Dames and Moore (1988) The upper two sub-basins were equipped with runoff measuring stations, namely, J415 and J417. From these reports, simultaneous measurements for both rainfall storms and runoff were collected. Al-Lith dam was constructed later at station J417 (to be completed in year 2020). Table 4 gives the characteristics of the dam and spillway https://ar.wikipedia.org/wiki/Al-Lith_Dam. The present study is dealing with those two sub-basins. Geologically, wadi Al-Lith is underlain by late Proterozoic plutonic, metavolcanic, and metasedimentary rocks in most of the wadi with an area about 86.8% of the total area, by chiefly Tertiary sedimentary, volcanic, and plutonic rocks in and near the coastal plain and by Tertiary oceanic crust of the Red Sea offshore. The contact between continental and oceanic crust is probably 10–15 km on-shore. Quaternary sediments of aeolian silt and pediment deposits with area of about 12% of the total area blanket the coastal plain with thickness that ranges from 2 to 10 m and fringed by coral reefs that are uplifted locally along faults parallel to the coast.

To further test the two reservoir models, three recorded runoff hydrographs at station J417 are routed over the dam using the two reservoir models in addition to the traditional method (modified Plus method) as a reference. Figure 4 shows the results of the routing calculations. The figure shows that the logarithmic model performs better than the power law model. The % of error estimation for both peak flow and volume are given by,

$$E_Q = \frac{Q_{\max}(\text{traditional}) - Q_{\max}(\text{method})}{Q_{\max}(\text{traditional})} \times 100 \tag{12}$$

$$E_V = \frac{V(\text{traditional}) - V(\text{method})}{V(\text{traditional})} \times 100 \tag{13}$$

where E_Q is the percentage of error in peak discharge, $Q_{\max}(\text{traditional})$ is the peak discharge from the traditional method, and $Q_{\max}(\text{method})$ is the peak discharge from the logarithmic or power law method. In Eq. (13), E_V is the percentage of error in volume, $V(\text{traditional})$ is the volume from the traditional method, and $V(\text{method})$ is the volume from the logarithmic or power law method.

The error estimation is shown in Table 5, which shows that the percentage of error for the power law is higher than that of the logarithmic model. It also shows the attenuation ratio (in-flow peak divided by the outflow peak), which supports the same conclusion that the logarithmic method performs better than the power law method.

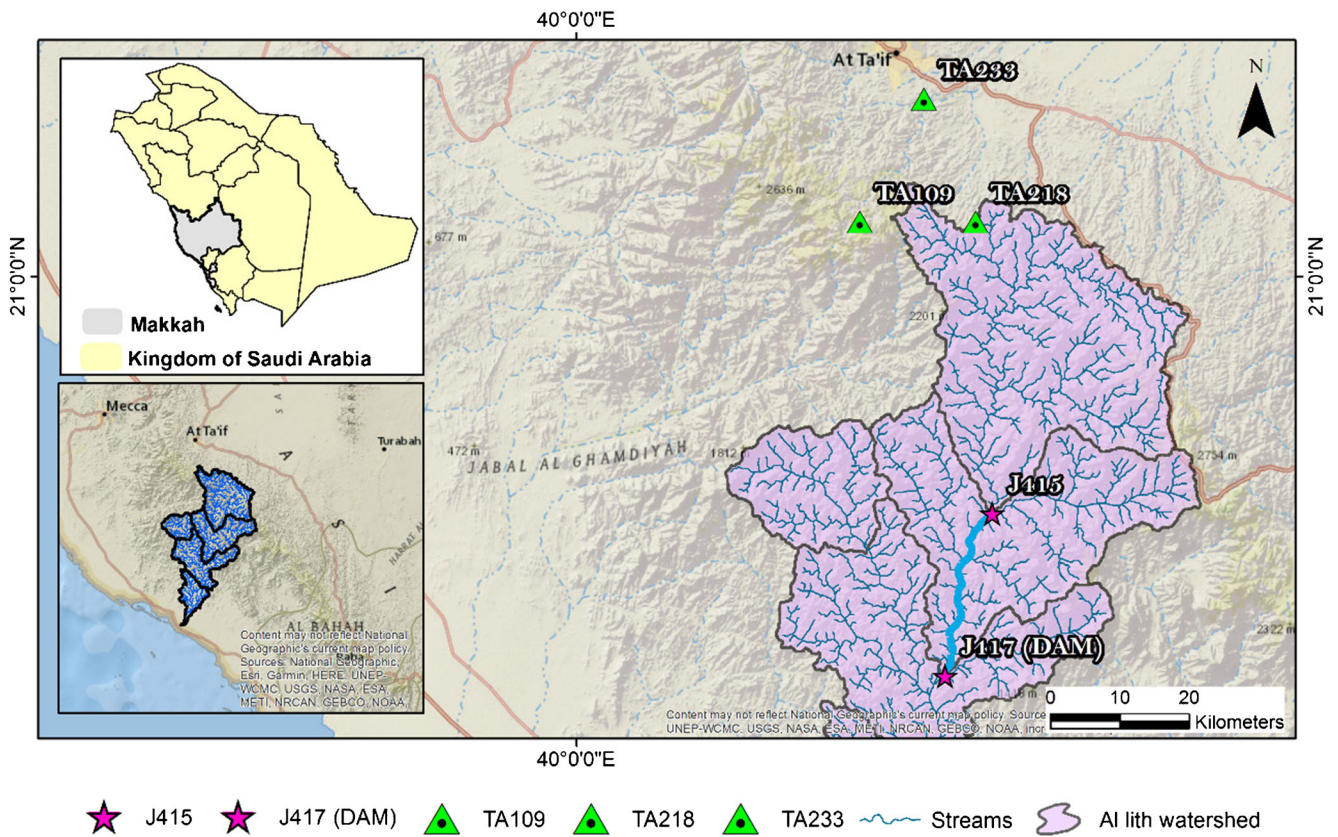


Fig. 3 Location of the case study: Al-Lith dam and its basin

Rainfall analysis based on recorded data up to 2019

Three rainfall stations, namely, TA109, TA218, and TA233, are selected. Table 6 shows the characteristics of these stations. The usual statistical analysis (Kite 1975) calls for fitting the data from each station to common distributions and select the best fit based on an error criterion then run spatial analysis to obtain the design storm for each sub-basin for further hydrological analysis. However, there were two problems with the available data: first, the number of records of the three stations was different and, second, the storms are usually local and do not cover the entire area of the watersheds. Following the method suggested by Wheater et al. (1989), an average of the records of the three stations was calculated and then the best distribution, Gumbel in this case, is fitted to the data. Table 7 shows the results of this analysis as the expected rainfall depths for various return periods.

Table 4 Characteristics of Al-Lith dam and its spillway

Dam		Spillway	
Height of dam (m)	44.5	Height of spillway (m)	37
Length of dam (m)	420	Length of spillway (m)	350
Capacity (m ³)	90,000,000		

Unit hydrograph of wadi Al-Lith

Transformation of rainfall data into runoff was carried out by performing hydrologic analysis with the aid of the commonly used hydrological modeling system (HEC 2000). The HEC-HMS software (US Army Corps of Engineers HEC-HMS (n.d.)) is used to determine the relationship between rainfall and runoff of the catchment, which allows the user to select between numerous losses and hydrograph parameterization such as the Soil Conservation Services curve number (SCS-CN) scheme. The software also allows to employ user-defined unit hydrograph and hyetograph. Albishi et al. (2017) presented 1-h unit hydrograph for Al-Lith basin as well as for stations J415 and J417. The 1-h unit hydrographs for both stations are used later with the design storm to predict the inflow hydrograph at the dam site.

Transmission losses in ephemeral streams

Since transmission loss is one of the key phenomena in arid regions, it should be considered in the analysis of the flood routing between stations J415 and J417. These stations, as shown in Fig. 3 and Table 8, present the characteristics of the stations. The three-parameter Muskingum method (O'Donnell 1985) is used for the estimation of transmission losses. Elfeki et al. (2014) gave the three-

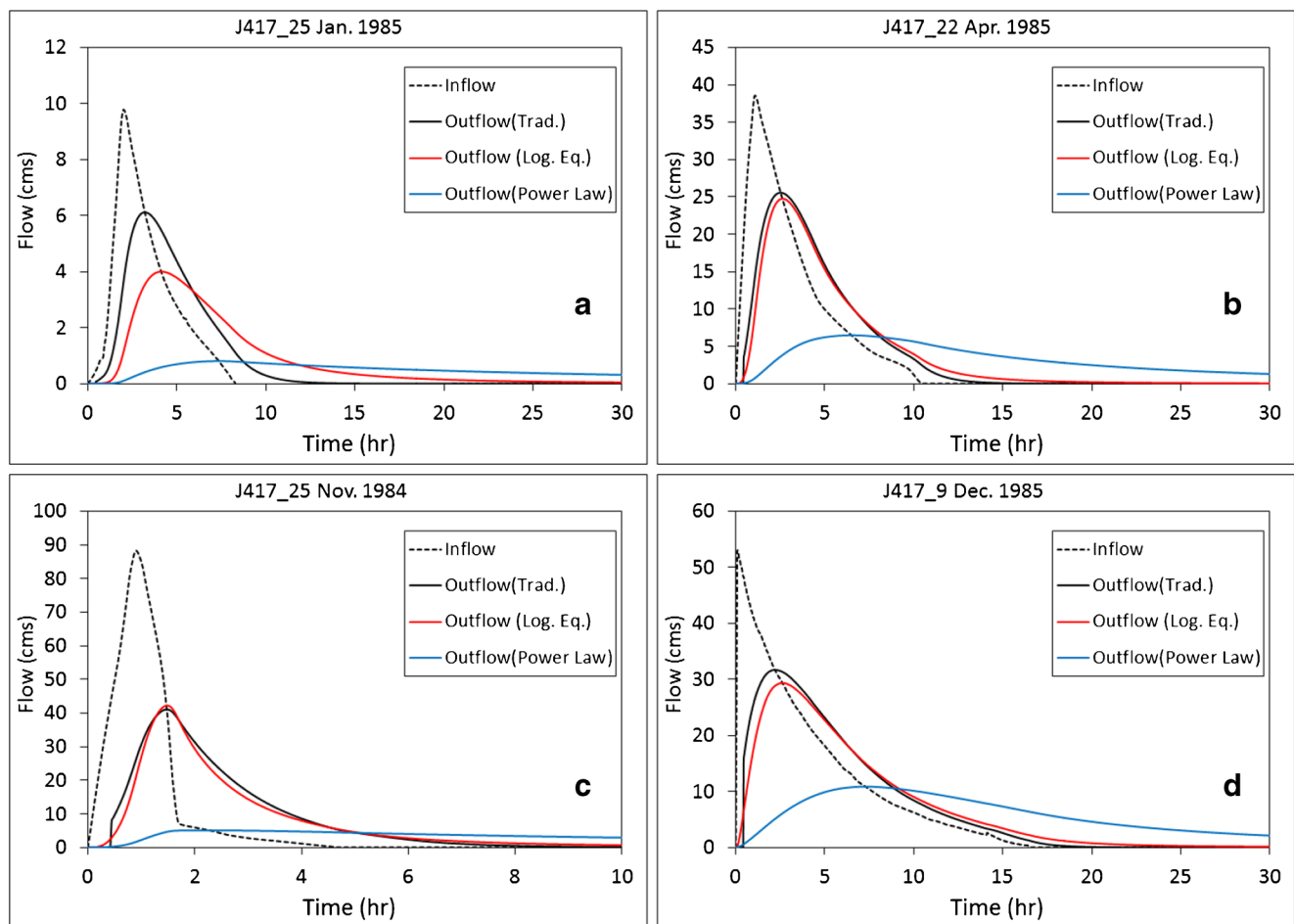


Fig. 4 Comparison between reservoir routing for the two reservoir models and the traditional Plus method based on some real flood storms: **a** 25/1/1985; **b** 22/4/1985; **c** 25/11/1984; and **d** 9/12/1985

parameter Muskingum routing equation that incorporates transmission losses as

$$O'(t + \Delta t) = d_1 I'(t) + d_2 I'(t + \Delta t) + d_3 O'(t) \tag{14}$$

where $I(t)$ is the inflow hydrograph at the channel reach (station J415) at time t (Fig. 3), $O'(t)$ is the outflow hydrograph at station J417 at time t (Fig. 3), $I'(t + \Delta t)$ is the inflow hydrograph at the channel reach (station J415) at time $t + \Delta t$ (Fig. 3), $O'(t + \Delta t)$ is the outflow hydrograph

at station J417 at time $t + \Delta t$ (Fig. 3), and $d_1, d_2,$ and d_3 are fitting parameters.

The fitting parameters can be estimated by the matrix inversion least squares solution for the given inflow and outflow hydrographs at the two stations. The channel reach parameters, $K, \alpha,$ and $x,$ can be estimated using the formulas below (O'Donnell 1985; O'Donnell et al. 1988):

$$K = \Delta t \frac{d_1 + d_2 d_3}{(1 - d_3)(d_1 + d_2)} \tag{15}$$

Table 5 Results of the outflow routed hydrographs from both reservoir models and the traditional modified Plus method

Date	Total rainfall (mm)	Traditional Plus method			Logarithmic method				Power method					
		Q_{max} (m ³ /s)	Att. Ratio	Volume (m ³)	Q_{max} (m ³ /s)	Att. ratio	% E_Q	Volume (m ³)	% E_V	Q_{max} (m ³ /s)	Att. ratio	% E_Q	Volume (m ³)	% E_V
25/11/1984	21.5	41.12	0.47	343,855	42.29	0.48	-2.84	339,991	1.12	5.08	0.06	87.66	332,037	3.44
25/1/1985	17.7	6.11	0.62	100,756	4	0.41	34.53	100,713	0.04	0.81	0.08	86.74	154,725	-53.56
22/4/1985	13.2	25.57	0.66	493,991	24.76	0.64	3.18	493,959	0.01	6.49	0.17	74.63	452,460	8.41
9/12/1985	29.8	31.68	0.60	830,859	29.33	0.55	7.44	830,805	0.01	10.86	0.20	65.73	779,255	6.21

Table 6 Rainfall stations used for estimation of the design storms

Stations	Coordinates		Period	No. of record (years)
	Easting	Northing		
TA109	40° 22' 4.41"	21° 3' 59"	1964–2019	56
TA218	40° 31' 4.41"	21° 3' 59"	1966–2018	53
TA233	40° 27' 4.4"	21° 12' 59"	1971–2006	36

$$x = 0.5 \left(1 - \frac{d_2 + d_2 d_3}{d_1 + d_2 d_3} \right) \quad (16)$$

$$\alpha = \frac{d_1 + d_2 + d_3 - 1}{1 - d_3} \quad (17)$$

where K is the channel time lag (the hydrograph movement time), x is a weighting parameter, and α is the coefficient of lateral flow, which accounts for the transmission losses in ephemeral stream.

The estimation of the parameters of the channel reach between stations J415 and J417 was performed based on the three recoded events at the wadi sub-basins at stations J415 and J417. Figure 5 shows the results of the flood routing technique between the two stations. Very good agreement can be observed between the observed and reconstructed outflow. A quantitative analysis of the fitting is presented in Table 9. The RMSE (root mean square error) shows a maximum value of 0.72 m³/s, which is relatively low and acceptable from the engineering perspective.

The estimated model parameters are tabulated in Table 10. The average of these parameters show 25% transmission losses from the inflow hydrograph and the time lag between the two stations is about 1.4 h, and the weighting parameter for the channel storage estimation is 0.032. These parameters are used in the predictions of the flood routing of the design storms.

Climate change effect on the hydrological regime

The Rossby Centre regional atmospheric climate model (RCA), originally developed by the Swedish Meteorological and Hydrological Institute (SMHI), has downscaled two

Table 7 Predicted design storm (based on Gumbel distribution)

Return period	Probability	Prediction (mm)
5	0.8	50.36
10	0.9	60.35
25	0.96	72.97
50	0.98	82.34
100	0.99	91.63

Table 8 Some main features of the runoff stations at Al-Lith basin

Station	Easting	Northing	Area (km ²)	Length of the main stream (km)	Slope (m/m)	Channel reach length (km)
J415	42° 32' 21.27"	20° 42' 49.61"	974.8	85.4	0.3332	25.1
J417	40° 28' 44.05"	20° 30' 56.69"	735.2	61.4	0.3491	

Coupled Model Intercomparison Project 5 (CMIP5) global climate models (GCMs; Meehl et al. 2007; Taylor et al. 2012). These are the Centre National de Recherches Météorologiques (CNRM-CM5) and the NOAA Geophysical fluid Dynamics Laboratory (GFDL-ESM2M), under the COordinated Regional climate Downscaling EXperiment (CORDEX; Strandberg et al. 2014; Giorgi et al. 2009) framework for Middle East North Africa (MENA) domain (Moss et al. 2010). The CORDEX RCA4 outputs of precipitation for the MENA simulations cover the study domain with horizontal grid resolution of 0.44° × 0.44° which corresponds to approximately 50 × 50 km grid spacing. In this study, the fourth version of the RCA4 (Samuelsson et al. 2015), driven by CNRM-CM5 GCM, model is used for investigating the effects of future climate change on the maximum daily rainfall over the three stations, viz. TA109, TA233, and TA218. Further details on RCA4 model's background, physical processes, development, and application since it was established can be found in the following literature (see, for instance, Samuelsson et al. 2015; Samuelsson et al. 2011; Kjellström et al. 2011; Räisänen et al. 2004; Jones et al., 2004a, b; Rummukainen et al. 2001). Furthermore, the detailed information about CORDEX domains, experiment guidelines, data access, list of RCMs, GCMs and variables, etc. are available at the following weblink: <https://cordex.org/data-access/cordex-data-on-esgf/>. A recent study conducted by Syed et al. (2019) showed that the RCA4 simulations forced with CNRM-CM5 GCM lateral boundary conditions well approximate the observations, therefore have been selected for the current study. The baseline RCA4 model outputs are calibrated, following Ahmad and Rasul (2018), by fitting the data into five different distributions/transformations (PTF, DIST, RQUANT, QUANT, and SSPLIN) for the periods 1964–2005, 1971–2005, and 1980–1991 for TA109, TA233, and TA218 stations, respectively. The transformations for the selected three stations are carefully examined for the abovementioned baseline periods with their associated stations using RCA4 model output statistics and biases in respective quantiles. To select the best transformation/distribution in the models' historical simulations, the mean, standard

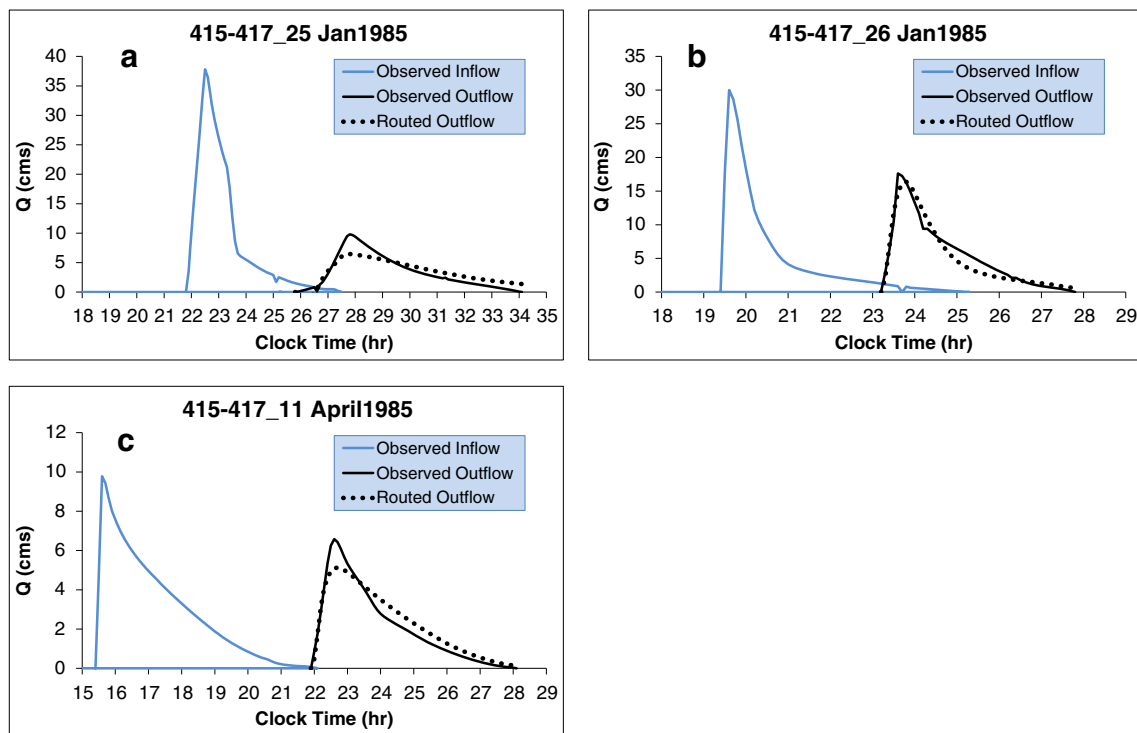


Fig. 5 a–c Comparison between observed and reconstructed hydrographs routed for stations J415 and J417 for three events that cover the two stations for the estimation of the three parameters of the Muskingum method

deviation, coefficient of variation, and coefficient of skewness are compared with the observations (Table 11). Therefore, the distribution/transformation with the least bias is selected for the historical run for each of the station. Using the selected distribution, the future projections are then empirically adjusted and downscaled to station level for the future period 2006–2100 under both RCP4.5 and RCP8.5 scenarios. Figure 6 shows the results of the two scenarios compared with the observed data. Statistical analysis employing Gumbel distribution on the observed data and the predicted results are conducted and presented in Fig. 7 for the two scenarios. The results show that the predicted rainfall from scenario RCP4.5 increased by 19.7 to 31.4% from 5 to 100 years return periods respectively with an average of 27%. While for scenario RCP8.5, the predicted rainfall increased by 42 to 55% from 5 to 100 years return periods respectively with an average of 49%.

Table 9 Observed versus calculated peak flow of the routed hydrograph and the RMSE of the fitting

Reach	Date	Q_p (Obs.) (m ³ /s)	Q_p (routed) (m ³ /s)	RMSE (m ³ /s)
Inflow J415	25-Jan-85	9.8	6.5	0.72
outflow J417	26-Jan-85	17.6	16.4	0.46
	11-Apr-85	6.0	5.1	0.230

Based on the frequency analysis for the two climate change scenarios (RCP4.5 and RCP8.5), hydrographs for 5, 10, 25, 50, and 100 years return periods are estimated and depicted in Fig. 8 taking into consideration the effect of transmission losses. Figure 8a shows the generated hydrographs based on the current rainfall data records, while Fig. 8b, c shows the generated hydrographs based on the climate change scenarios RCP4.5 and RCP8.5, respectively. Table 12 shows a comparison between peak discharges and runoff volumes for the observed data and the two climate change scenarios for different return periods under the condition that there is no transmission losses included. The table shows that, for the RCP4.5 scenario, the peak flows increased between 65% and 71% with an average of 69%, while the runoff volume increased between 63% and 68% with an average of 67%. For the RCP8.5

Table 10 Estimation of the Muskingum routing parameters from the recorded events

Reach	Date	Estimated values			K (h)	x	α
		d_1	d_2	d_3			
Inflow J415	25-Jan-85	0.089	-0.069	0.970	3.64	0.110	-0.35
outflow J417	26-Jan-85	0.111	0.116	0.732	0.32	-0.004	-0.15
	11-Apr-85	0.093	0.100	0.741	0.335	-0.010	-0.254
Average		0.098	0.049	0.814	1.432	0.032	-0.251

Table 11 Comparison between the observed and predicted statistics based on RCP4.5 and RCP8.5 scenarios

Properties	TA109			TA218			TA233		
	Observed	RCP4.5	RCP8.5	Observed	RCP4.5	RCP8.5	Observed	RCP4.5	RCP8.5
Mean	44.94	42.75	52.95	26.26	49.51	72.09	47.33	38.79	51.71
Standard deviation	20.60	18.66	21.15	31.02	40.53	52.15	29.32	22.98	28.69
Coefficient of variation	0.46	0.44	0.40	1.18	0.82	0.72	0.62	0.59	0.55
Coefficient of skewness	0.75	0.78	0.72	2.02	1.77	0.99	1.07	1.32	1.18

scenario, the peak flows increased between 128% and 151% with an average of 139%, while the runoff volume increased between 123% and 147% with an average of about 134%. Table 13 shows the same comparison as Table 12, but with

inclusion of transmission losses in the wadi. The table shows that, for RCP4.5 scenario, the peak flows increased between 63% and 70% with an average of about 67%, while the runoff volume increased between 62% and 69% with an average of

Fig. 6 Comparison between two climate change scenarios with the observed data for the three rainfall stations

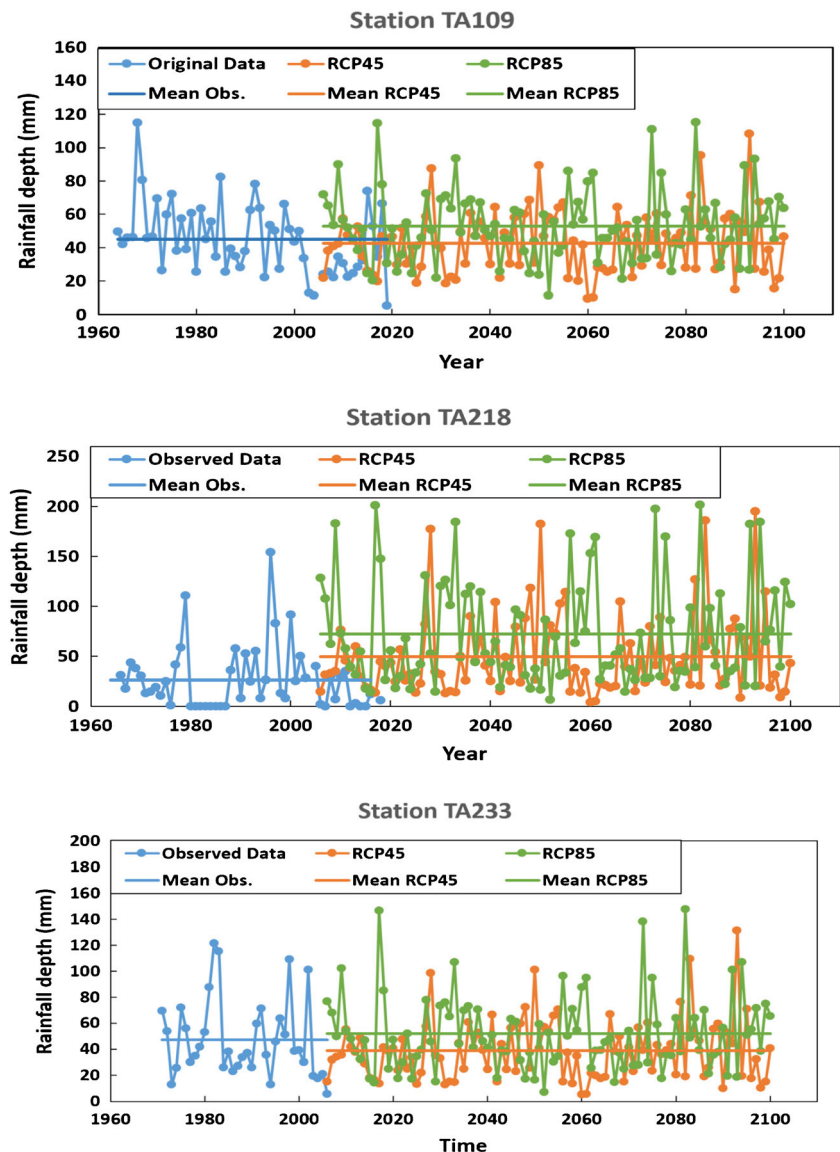
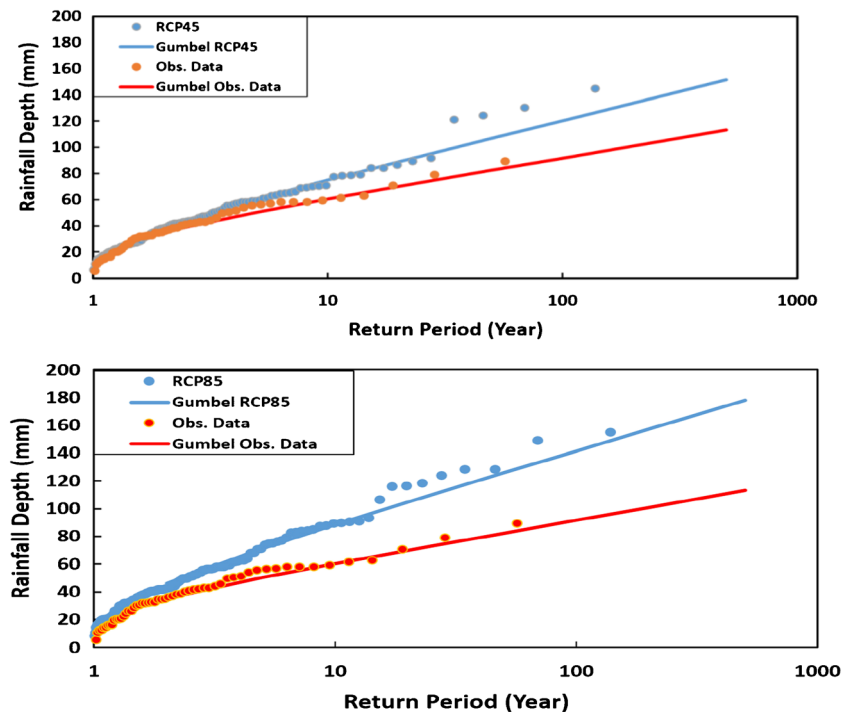


Fig. 7 Frequency analysis for both the observed data and the two scenarios of climate change



about 67%. For RCP8.5 scenario, the peak flows increased between 125% and 146% with an average of the order 134%, while the runoff volume increased between 123% and 149% with an average of about 134%.

The results show that for the RCP4.5 scenario without transmission losses, the flood volume for the 100 years return period is safe within the maximum capacity of the reservoir. While for the RCP8.5 scenario without transmission losses, the volume of the 50 years return period will exceed the reservoir capacity. For the RCP4.5 scenario with transmission losses, the flood volume for the 100 years return period is safe within the maximum capacity of the reservoir. While for the RCP8.5 scenario with transmission losses, the volume of the 100 years return period will exceed the reservoir capacity. Therefore, the design of the flood mitigation infrastructures must take into account the climate change effects on the rainfall-runoff analysis.

Conclusions

The following conclusions can be drawn from the study:

- (1) Classification of the 136 dams' reservoirs, based on Borland and Miller (1958) criteria, shows that the majority of the reservoirs (75%) fall in class III, i.e., flood plain foothill.
- (2) The two models adopted for representing the reservoir morphology, namely, the power and logarithmic laws, show that the percentage of error for the logarithmic law is between -4 and +8% while for the power law, the range is between -50 and +5%. In addition, R^2 was higher for the logarithmic law. The range of the %RRMSE for the logarithmic method lies between 5.1 and 7.7% with an average of 6.6%, while for the power method, the range is between 15 and 24.9% with an average of 22.7%. These results indicate that the logarithmic law performs much better than the power law. Therefore, it is recommended to use the logarithmic law in the dam design in the study area.
- (3) The transmission losses, estimated by the three-parameter Muskingum method, show that the average transmission losses are 25% between the two stations under study. This value should be considered in the design of mitigation measures in the study area.
- (4) Two future climate change scenarios, i.e., RCP4.5 and RCP8.5, of the Rossby Centre regional climate model (RCA4) run with CNRM-CM5 GCM boundary conditions under CORDEX framework for MENA domain are used in the present study. The results reveal that, in terms of mean, standard deviation, coefficient of variance, and skewness, the changes from the current properties are not pronounced. However, as far as frequency analysis is

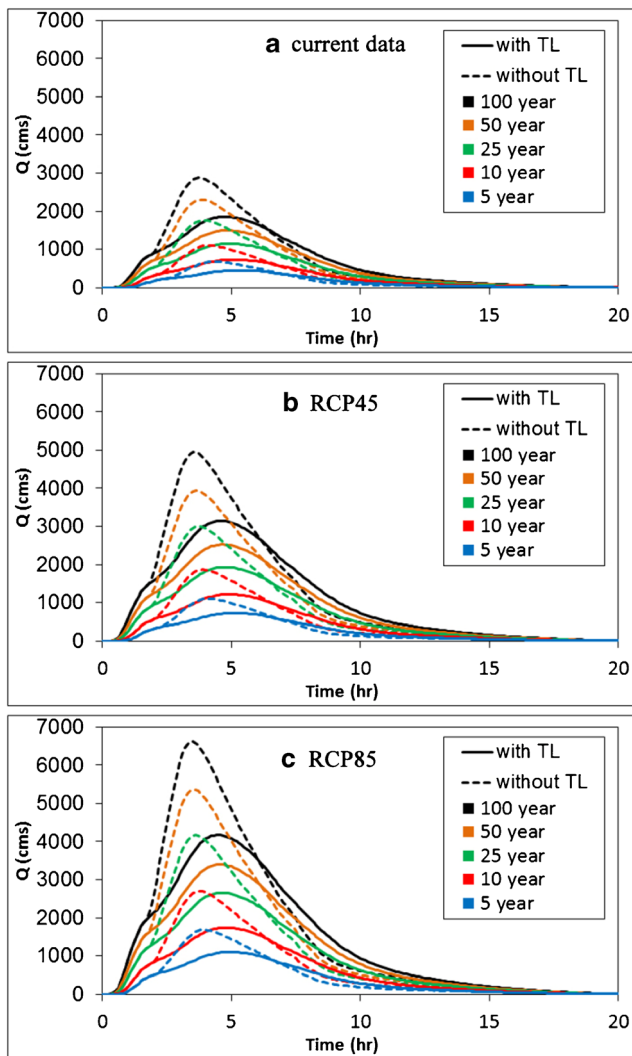


Fig. 8 Inflow hydrographs at the dam site for 5, 10, 25, 50, and 100 years return periods with and without transmission losses for the current data and the two climate change scenarios: **a** current data, **b** CCRC4.5, and **c** CCRC8.5

- considered, the rainfall peak flows and runoff volumes of predicted hydrographs for all return periods show very pronounced increase.
- (5) The results also show that the predicted rainfall from scenario RCP4.5 increased by about 20 to 31% from 5 to 100 years return periods, respectively, with an average of about 27%. While for RCP8.5 scenario, the predicted rainfall increased by 42 to 55% from 5 to 100 years return periods, respectively, with an average of about 49%.
 - (6) For the RCP4.5 scenario, the peak flows and volumes increased by an average of 69% and 67%, respectively, in the case of no transmission losses included. However, in the case of transmission losses included, the peak flows and runoff volumes increased by an average of 67% and 67%, respectively. For RCP8.5 scenario, the peak flows and runoff volumes increased by an average of 139% and 134%, respectively, in case of no transmission losses included. However, in the case of transmission losses included, the peak flows and runoff volumes increased by an average of 134% and 134%, respectively.
 - (7) The effect of transmission losses in the results seem to be minor with respect to climate change signal (for RCP4.5, Q and V are lowered on average by 2% and 0.5%, respectively, and for RCP8.5, Q and V are lowered on average by 4.5% and 1.3% respectively).
 - (8) The results show that for the case with transmission losses, the runoff volume for the 100 years return period exceeds the design capacity of the dam under the RCP4.5 scenario. While under the RCP8.5 scenario, the runoff volumes for the 50 and 100 years return periods exceed the design volume of the dam. Therefore, the effect of the climate change must be taken into account in the design of the flood mitigation infrastructures.

Table 12 Comparison between peak flows and runoff volumes without transmission losses of the observed data and the two climate change scenarios for return periods 5, 10, 25, 50, and 100 years

Return periods	Observed data		RCP4.5			RCP8.5				
	Q (cms)	Volume (m ³)	Q (cm)	Volume (m ³)	% change		Q (cms)	Volume (m ³)	% change	
					Q	Volume			Q	Volume
5	668.2	12.09	1102.5	19.75	65.00	63.42	1680.2	29.89	151.45	147.30
10	1103.0	19.76	1863.0	33.06	68.90	67.31	2697.5	47.48	144.56	140.26
25	1756.7	31.24	3000.8	52.64	70.82	68.48	4166.1	72.40	137.15	131.72
50	2306.6	40.79	3944.0	68.70	70.99	68.43	5362.6	92.47	132.49	126.72
100	2895.7	50.86	4945.9	85.56	70.80	68.23	6619.4	113.36	128.59	122.89

Table 13 Comparison between the peak flows and volumes with transmission losses of the observed data and the two climate change scenarios for return periods 5, 10, 25, 50, and 100 years

Return periods	Observed data		RCP4.5			RCP8.5				
	Q (cm)	Volume (m ³)	Q (cm)	Volume (m ³)	% change		Q (cm)	Volume (m ³)	% change	
					Q	Volume			Q	Volume
5	446.2	10.66	725.7	17.28	62.64	62.10	1096.4	26.06	145.72	144.47
10	726.9	17.31	1212.3	28.8	66.78	66.38	1741.4	41.26	139.57	138.36
25	1145.8	27.25	1930.5	45.71	68.48	67.74	2659.3	62.75	132.09	130.28
50	1492.4	35.43	2521.9	59.56	68.98	68.22	3400.7	80.04	127.87	125.91
100	1852.5	43.88	3144.4	74.08	69.74	68.87	4175.4	98.01	125.39	123.36

Acknowledgments The authors, therefore, acknowledge with thanks the DSR for technical and financial support. The authors also would like to thank Mr. Abdullah Almalki for the preparation of the graphs.

Funding information This project was funded by the Deanship of Scientific Research (DSR), King Abdulaziz University, Jeddah, under grant no. (G-158-155-1440).

Compliance with ethical standards

Conflict of interest The authors declare that they have no competing interests.

Appendix

The mass conservation equation for reservoir routing is given by the following:

$$\frac{dW(t)}{dt} = I(t) - O(t), \tag{18}$$

where $W(t)$ is the storage of the reservoir, $I(t)$ is the inflow hydrograph upstream the dam, and $O(t)$ is the outflow hydrograph downstream the dam passed over the spillway.

The spillway equation reads as follows:

$$O(t) = CB[Z - P]^{1.5} \text{ if } Z > P \tag{19}$$

$$O(t) = 0 \text{ if } Z \leq P \tag{20}$$

where C is the discharge coefficient, B is the spillway width, Z is water depth measured from the reservoir bottom, and P is the spillway height measured from the reservoir bottom.

The storage term in Eq. (18) is required to be assessed. This term can be rewritten as follows:

$$\frac{dW(t)}{dt} = \frac{dW(t)}{dZ} \frac{dZ}{dt} = A(Z) \frac{dZ}{dt} \tag{21}$$

where $A(Z)$ is the surface area of the reservoir. Substituting Eq. (21) in Eq. (18) yields the following:

$$\frac{dZ}{dt} = \frac{I(t) - O(t)}{A(Z)} \tag{22}$$

The two methods presented earlier (the power law and the logarithmic law) are used to quantify the surface area of the reservoir by differentiating Eqs. (1) and (2). Then substituting in Eq. (22) including Eqs. (19) and (20) for the reservoir outlet yields the following equations for the power law and the logarithmic law respectively presented in the paper (Eqs. 8 and 9).

References

Ahmad B, Rasul G (2018) Statistically downscaled projections of CORDEX South Asia using quantile mapping approach over Pakistan region. *Int J Global Warming* 16(4):435–460

Albishi M, Bahrawi J, Elfeki A (2017) Derivation of the unit hydrograph of Al-lith basin in the south west of Saudi Arabia. *Int J Water Res Environ* 6(1):50–57

Ambjerg-Nielsen K (2012) Quantification of climate change effects on extreme precipitation used for high resolution hydrologic design. *Urban Water J* 9(2):57–65

Borland WM, Miller CR (1958) Distribution of sediment in large reservoirs. *J Hydraul Div* 84(2):1587.1–1587.10

Chow VT, Maidment DR, Mays LW (1988) *Applied hydrology*, international editions. McGraw-Hill, New York, pp 242–251

Chowdhury S, Al-Zahrani M (2013) Implications of climate change on water resources in Saudi Arabia. *Arab J Sci Eng* 38:1959–197. <https://doi.org/10.1007/s13369-013-0565-6>

Dames and Moore (1988) Representative basins study for wadis: Yiba, Habawnah, Tabalah, Liyyah, and Lith, Draft final report to the Ministry of Agriculture and Water, Kingdom of Saudi Arabia, Riyadh

Elfeki AM, Ewea HAR, Bahrawi JA, Al-Amri NS (2014) Incorporating transmission losses in flash flood routing in ephemeral streams by using the three-parameter Muskingum method. *Arab J Geosci* 8: 5153–5165. <https://doi.org/10.1007/s12517-014-1511-y>

- Elshorbagy A, Lindenas K, Azinfar H (2018). Risk-based quantification of the impact of climate change on storm water infrastructure, 32(1), 102–114
- Giorgi F, Jones C, Asrar GR (2009). Addressing climate information needs at the regional level: the CORDEX framework. World Meteorological Organization (WMO) Bulletin, vol. 58, no. 3, pp. 58, 175
- HEC (2000) Hydrologic modeling system: technical reference manual. US Army Corps of Engineers Hydrologic Engineering Center, Davis
- Haghiabi AH, Salmian SS, Mohammadzadeh-Habili J, Mousavi SF (2013) Derivation of reservoir's area-capacity equations based on the shape factor. *Trans Civil Eng* 37(C1):163–167
- Jones CG, Ullerstig A, Willén U, Hansson U (2004a) The Rossby Centre regional atmospheric climate model (RCA). Part I: model climatology and performance characteristics for present climate over Europe. *Ambio* 33(4–5):199–121
- Jones RG, Noguier M, Hassell DC (2004b) Generating high-resolution climate change scenarios using PRECIS. Exeter, Met Office Hadley Centre
- Kamis AS, Bahrawi JA, Elfeki AM (2018) Reservoir routing in ephemeral streams in arid regions. *Arab J Geosci* 11(6):106
- Kite GW (1975) Confidence limits for design events. *Water Resour Res* 11(1):48–53
- Kjellström E, Nikulin G, Hansson U, Strandberg G, Ullerstig A (2011) 21st century changes in the European climate: uncertainties derived from an ensemble of regional climate model simulations. *Tellus A: Dynamic Meteorol Oceanogr* 63(1):24–40
- Li M, Tang X, Wu W, Liu H (2013) General models for estimating daily global solar radiation for different solar radiation zones in mainland China. *Energy Conserv Manag* 70:139–148
- Macchione F, De Lorenzo G, Costabile P, Rezdar B (2016) The power function for representing the reservoir rating curve: morphological meaning and suitability for dam breach modeling. *Water Resour Manag* 30(13):4861–4881
- Meehl GA, Covey C, Delworth T, Latif M, McAvaney B, Mitchell JFB (2007) The WCRP CMIP3 multi-model dataset: a new era in climate change research. *Bull Am Meteorol Soc* 88(9):1383–1394
- Mohammadzadeh-Habili J, Heidarpour M, Mousavi S, Haghiabi AH (2009) Derivation of reservoir's area capacity equations. *J Hydrol Eng* 14:1017–1023
- Moore D. (1998). Representative basins study for wadis: Yiba, Habawnah, Tabalah, Liyyah and Lith, Final Report by Dames & Moore, Saudi Arabia to Ministry of Agriculture and Water, Riyadh, 1988
- Moss RH, Edmonds JA, Hibbard KA, Manning MR, Rose SK, Van Vuuren DP, Carter TR, Emori S, Kainuma M, Kram T, Meehl GA, Mitchell JFB, Nakicenovic N, Riahi K, Smith SJ, Stouffer RJ, Thomson AM, Weyant JP, Wilbanks TJ (2010) The next generation of scenarios for climate change research and assessment. *Nature* 463(7282):747–756
- O'Donnell T (1985) Direct three-parameter Muskingum procedure incorporating lateral inflow. *Hydrol Sci J* 30(4):479–496
- O'Donnell T, Pearson CP, Woods RA (1988) Improved fitting for three-parameter Muskingum procedure. *J Hydraul Eng* 114(5):516–528
- Monier E, Gao X (2015) Climate change impacts on extreme events in the United States: an uncertainty analysis. *Clim Chang* 131(1):67–81
- Rahmanian MR, Banihashemi MA (2012) Introduction of a new empirical shape function to define sediment distribution pattern in dam reservoirs. *Trans Civil Eng* 36(C1):79–92
- Räisänen J, Hansson U, Ullerstig A, Döscher R, Graham LP, Jones C (2004) European climate in the late 21st century: regional simulations with two driving global models and two forcing scenarios. *Climate Dynam* 22:13–31
- Rajab R, Prudhomme C (2002) Climate change on water resources management in arid and semi-arid regions: prospective and challenges for the 21st century. *Biosyst Eng* 81(1):3–34
- Rummukainen M, Räisänen J, Bringfelt B, Ullerstig A, Omstedt A, Willén U (2001). A regional climate model for northern Europe: model description and results from the downscaling of two GCM control simulations. *Climate Dynamics*, vol. 17, no. 5–6, pp. 17: 339–359
- Samuelsson P, Gollvik S, Kupiainen M, Kourzeneva E, van de Berg WJ (2015) The surface processes of the Rossby Centre regional atmospheric climate model (RCA4). Norrköping, Sweden, SMHI, p 2015
- Samuelsson P, Jones CG, Willén U, Ullerstig A, Gollvik S, Hansson U, Jansson C, Kjellström E, Nikulin G, and Wyser K (2011). The Rossby Centre regional climate model RCA3: model description and performance, *Tellus Ser A* 63(1): 4–23
- Strandberg, G, Kjellström E, Poska A, Wagner S, Gaillard MJ, Trondman AK, Mauri A, Davis BAS, Kaplan J O, Birks HJB, Bjune A E, Fyfe R, Giesecke T, Kalnina L, Kangur M, van der Knaap WO, Kokfelt U, Kuneš P, Lata'lova M, Marquer L, Mazier F, Nielsen AB, Smith B, Seppä H, and Sugita, S (2014) Regional climate model simulations for Europe at 6 and 0.2 k BP: sensitivity to changes in anthropogenic deforestation. *Clim Past* 10:661–680. <https://doi.org/10.5194/cp-10-661-2014>
- Syed FS, Latif M, Al-Maashi A, Ghulam A (2019) Regional climate model RCA4 simulations of temperature and precipitation over the Arabian Peninsula: sensitivity to CORDEX domain and lateral boundary conditions. *Clim Dyn* 53(11):7045–7064
- Taylor KE, Stouffer RJ, Meehl GA (2012) An overview of CMIP5 and the experiment design. *Bull Am Meteorol Soc* 93(4):485–498
- US Army Corps of Engineers HEC-HMS <http://www.hec.usace.army.mil/software/hec-hms/>
- Wheater HS, Laurentis P, Hamilton GS (1989) Design rainfall characteristics for south-west Saudi Arabia. *ProcInstCivEng* 87(4):517–538